Preparation of KOH and H3PO4 Modified Biochar and Its Application in Methylene Blue Removal from Aqueous Solution

Authors:

Li Liu, Yang Li, Shisuo Fan

Date Submitted: 2020-01-07

Keywords: Adsorption, Methylene blue, H3PO4 modification, KOH modification, corn stalk biochar

Abstract:

Improperly treated or directly discharged into the environment, wastewater containing dyes can destroy the quality of water bodies and pollute the ecological environment. The removal of dye wastewater is urgent and essential. In this study, corn stalk was pyrolyzed to pristine biochar (CSBC) in a limited oxygen atmosphere and modified using KOH and H3PO4 (KOH-CSBC, H3PO4-CSBC, respectively). The biochars were characterized by surface area and pore size, X-ray diffraction (XRD), Fourier transform infrared (FTIR) spectroscopy, X-ray photoelectron spectroscopy (XPS), as well as their behavior in adsorbing methylene blue (MB). Results indicated that the pore structure of CSBC became more developed after modification by KOH. Meanwhile, H3PO4-CSBC contained more functional groups after activation treatment. The pseudo-second-order kinetic and the Langmuir adsorption isotherm represented the adsorption process well. The maximum MB adsorption capacity of CSBC, KOH-CSBC, and H3PO4-CSBC was 43.14 mg g?1, 406.43 mg g?1 and 230.39 mg g?1, respectively. Chemical modification significantly enhanced the adsorption of MB onto biochar, especially for KOH-CSBC. The adsorption mechanism between MB and biochar involved physical interaction, electrostatic interaction, hydrogen bonding and ??? interaction. Hence, modified CSBC (especially KOH-CSBC) has the potential for use as an adsorbent to remove dye from textile wastewater.

Record Type: Published Article

Submitted To: LAPSE (Living Archive for Process Systems Engineering)

Citation (overall record, always the latest version):	LAPSE:2020.0031
Citation (this specific file, latest version):	LAPSE:2020.0031-1
Citation (this specific file, this version):	LAPSE:2020.0031-1v1

DOI of Published Version: https://doi.org/10.3390/pr7120891

processes

MDPI

Article

Preparation of KOH and H_3PO_4 Modified Biochar and Its Application in Methylene Blue Removal from Aqueous Solution

Li Liu [1], Yang Li [2] and Shisuo Fan [3,*]

[1] School of Physics and Electronic Engineering, Fuyang Normal University, Fuyang 236037, China; wenfan1986@163.com
[2] School of Environmental Science and Engineering, Guangdong University of Technology, Guangzhou 510006, China; linziyi_ly@163.com
[3] School of Resources and Environment, Anhui Agricultural University, Hefei 230036, China
* Correspondence: fanshisuo@ahau.edu.cn; Tel./Fax: +86-551-6578-6311

Received: 29 October 2019; Accepted: 25 November 2019; Published: 1 December 2019

Abstract: Improperly treated or directly discharged into the environment, wastewater containing dyes can destroy the quality of water bodies and pollute the ecological environment. The removal of dye wastewater is urgent and essential. In this study, corn stalk was pyrolyzed to pristine biochar (CSBC) in a limited oxygen atmosphere and modified using KOH and H_3PO_4 (KOH-CSBC, H_3PO_4-CSBC, respectively). The biochars were characterized by surface area and pore size, X-ray diffraction (XRD), Fourier transform infrared (FTIR) spectroscopy, X-ray photoelectron spectroscopy (XPS), as well as their behavior in adsorbing methylene blue (MB). Results indicated that the pore structure of CSBC became more developed after modification by KOH. Meanwhile, H_3PO_4-CSBC contained more functional groups after activation treatment. The pseudo-second-order kinetic and the Langmuir adsorption isotherm represented the adsorption process well. The maximum MB adsorption capacity of CSBC, KOH-CSBC, and H_3PO_4-CSBC was 43.14 mg g^{-1}, 406.43 mg g^{-1} and 230.39 mg g^{-1}, respectively. Chemical modification significantly enhanced the adsorption of MB onto biochar, especially for KOH-CSBC. The adsorption mechanism between MB and biochar involved physical interaction, electrostatic interaction, hydrogen bonding and π–π interaction. Hence, modified CSBC (especially KOH-CSBC) has the potential for use as an adsorbent to remove dye from textile wastewater.

Keywords: corn stalk biochar; KOH modification; H_3PO_4 modification; Methylene blue; Adsorption

1. Introduction

Wastewater from the textile industry typically contains dyes and has a high content of organic toxicants, high color, and strong resistance to biodegradation, photolysis and oxidation, and is potentially carcinogenic. If improperly treated or directly discharged into the environment, wastewater containing dyes can destroy the quality of water bodies and pollute the ecological environment [1]. Methylene blue (MB) is an important synthetic dye and was widely used in the field of chemical indicators, dyes, biological dyes and drugs. Wastewater containing MB can enter a water body through different pathways and cause serious harm to environmental and human health [2]. Therefore, the need is urgent to develop an effective, low cost, easily operated technology for MB wastewater treatment. Adsorption has been an important technology to remove MB from wastewater. The correct choice and preparation of an efficient adsorbent is the priority for effective application of adsorption technology.

Currently, biochar is attracting great attention due to the important function it provides in greenhouse gas emission reduction, soil carbon sequestration, pollutant control and solid waste

reclamation [3,4]. Biochar is the solid residue of an organic material that is pyrolyzed in the absence of oxygen or in a limited oxygen atmosphere. Because biochar can be made from a wide variety of raw materials, has a good adsorption capacity, and has large surface area, pore volume and abundant functional groups, many investigations have assessed the use of biochar as an adsorbent for removing pollutants from aqueous solution [5–9].

Compared with that of commercially available activated carbon, the adsorption effect of biochar needs to be improved. Techniques for achieving this improvement have become an areaof intense research activity. Activated or modified biochar has been prepared and applied to remove specific contaminants [10–12]. Activation methods include physical and chemical pathways. Physical activation can increase the surface area and improve the pore structure of biochar. Likewise, chemical activation can enrich the functional types of biochar and provide more binding sites for pollutant removal [13–16]. The preparation of highly effective adsorbents can provide a new option for the utilization of corn residues.

Research has shown that KOH and H_3PO_4 are commonly used biochar activators. Luo et al. [17] investigated the sorption of norfloxacin, sulfamerazine and oxytetracycline by KOH-modified biochar (from cassava waste). Bashir et al. [18] studied Cd removal by KOH-modified biochar (from rice straw). Huang et al. [19] reported removal of tetracycline by KOH-modified biochar (from poplar sawdust). Meanwhile, Chen et al. [20] revealed tetracycline removal by H_3PO_4-modified biochar (from rice straw and swine manure). Peng et al. [21] indicated that adsorption of Cu(II) and Cd(II) was enhanced by H_3PO_4-modified biochars (from pine sawdust). Zhao et al. [22] confirmed that Cr(VI) and organic contaminants could be co-removed by H_3PO_4-modified biochars. All of this research has shown that modification of biochar using KOH and H_3PO_4 is effective and feasible. However, comparison of the modification effect of KOH-biochar and H_3PO_4-biochar to facilitate pollutant removal has rarely been reported.

More than 250 million metric tons of corn (i.e., maize) residues are generated annually in China [23]. The utilization pathways for these residues include industrial materials, animal feed, fuel products and biomass energy [24]. However, some corn residue is disposed of by open-air burning, which not only pollutes the environment, but also wastes a valuable biomass resource. Hence, it is urgent to explore new ways to utilize these residues.

In this study, corn residue (specifically corn stalks) was chosen as the research object and was pyrolyzed to prepare pristine biochar. KOH and H_3PO_4 were used to modify the pristine biochar. Then, the pristine and modified biochars were applied to remove MB from wastewater. The research was expected to provide a basis for corn residue utilization and removal of MB dye from wastewater.

2. Materials and Methods

2.1. Materials and Reagents

Corn stalk was collected from the Anhui agricultural university's experimental farm. Analytically pure reagents (MB, KOH, HCl, NaOH and H_3PO_4) were purchased from Sinopharm Chemical Reagent Co. Ltd. (Shanghai, China) for use in the experiments.

2.2. Preparation of Biochar and Modified Biochar

First, the corn stalk was washed with deionized water and dried in an oven. After drying, the stalk was crushed and passed through a 100 mesh sieve and then stored for future experimentation. Last, the crushed corn stalk was pyrolyzed to pristine biochar at 500 °C in a muffle furnace under limited oxygen atmosphere. After washing several times with pure water, the biochar was dried in an oven (80 °C for 24 h). This procedure produced pristine corn stalk biochar (CSBC).

A weight of 6.0 g CSBC was put into each of two centrifuge tubes. A weight of 6.0 g KOH and 20 mL pure water was added to one tube. An amount of 6 mL H_3PO_4 and 20 mL ultrapure was added to the other tube. Then, the two tubes were placed on a shaker to fully oscillate for 24 h, after which

the tubes were removed and the biochars dried at 80 °C for 48 h. Then, each of the treated biochars was placed in an individual ceramic crucible, covered with a lid, and placed in a muffle furnace to activate the biochars. The activation temperature was 700 °C (generally, the biochar was prepared under 700 °C, and thus the activation temperature was chosen as 700 °C), which was attained at a heating rate of 10 °C/min and maintained for 2 h. Then, the crucibles were cooled to room temperature and the modified biochars were removed. Deionized water was used to remove impurities from the biochars by washing them several times until the pH of eluent reached neutrality. The washed biochars were dried in an oven for characterization and use in experiments. Hereafter, the KOH-treated and H_3PO_4-treated biochars are referred to as KOH-CSBC and H_3PO_4-CSBC, respectively.

2.3. Characterization

The pristine and modified biochars were characterized using various techniques. The surface area and pore sized of the biochars were measured using an automatic specific surface area and pore analyzer (Tristar II 3020M, Micromeritics Instrument Corporation, Norcross, GA, USA). The surface morphology of biochars was analyzed using scanning electron microscopy (SEM, S-4800, Hitachi, Japan). Fourier transform infrared spectroscopy (FTIR) was used with the KBr pellet technique to characterize the functional groups of biochars (FTIR, Nicolette is50, Thermo Fisher Scientific, Waltham, MA, USA). The minerals in biochars were detected by X-ray diffraction (XRD, D8 Advance, BrukerAXS GmbH, Karlsruhe, Germany). The surface elements, speciation and relative distribution of elements within the biochars were determined by X-ray photoelectron spectroscopy (XPS, ESCALAB 250, Thermo Scientific-VG Scientific, Waltham, MA, USA).

2.4. Adsorption Experiments

2.4.1. Influence of Solid-to-Liquid Ratio on Methylene Blue (MB) Adsorption

MB solution (30 mL) with a concentration of 50 mg L^{-1} was placed in 50 mL centrifuge tubes. A certain mass of pristine or modified biochar was weighed and added into the tubes to adjust the solid-to-liquid ratio at 0.5, 1.0, 2.0, 3.0 and 4.0 g L^{-1}. Then, the tubes were placed in a constant temperature shaker with a speed of 150 rpm for 24 h at 25 °C. The tubes were centrifuged for 10 min at a speed of 4000 rpm. The resulting supernatant was filtered through a 0.45 μm membrane, and the absorbance of the supernatant at the wavelength of 665 nm was measured using a spectrophotometer.

2.4.2. Influence of Initial pH of Solution on MB Adsorption

MB solution (30 mL) with a concentration of 100 mg L^{-1} was placed in 50 mL centrifuge tubes. The pH of the solutions was adjusted to 3.0, 5.0, 7.0, 9.0 and 11.0 using either 0.1M HCl or NaOH. A certain mass of pristine or modified biochar was added to the tubes to adjust the solid-to-liquid ratio at 0.5 g L^{-1}. The tubes were then processed as described in Section 2.4.1 (i.e., oscillation, centrifugation, filtration and absorbance determination).

2.4.3. Adsorption Kinetics

MB solution (100 mL) at a concentration of 50 mg·L^{-1}, 100 mg·L^{-1} or 200 mg·L^{-1} was added to each of three beakers. Then, 0.1 g CSBC, 0.1 g KOH-CSBC and 0.1 g H_3PO_4-CSBC was added separately to each beaker. Each beaker was placed on a magnetic stirrer and the temperature held constant at 25 °C. Samples were collected at various times and filtered through a 0.45 μm membrane, after which the absorbance at 665 nm was detected. The concentration of MB was set at 50 mg L^{-1} and 100 mg L^{-1} for CSBC, and 100 mg L^{-1} and 200 mg L^{-1} for both KOH-CSBC and H_3PO_4-CSBC.

2.4.4. Adsorption Isotherm

To develop adsorption isotherms, 30 mL of MB solution was placed in a 50 mL centrifuge tube. The concentration of MB was adjusted in the range 100–500 mg·L^{-1}. Then, 0.015 g of CSBC, KOH-CSBC

and H_3PO_4-CSBC was added separately to individual tubes. The tubes were placed in a constant temperature shaker with a speed of 150 rpm for 24 h at 25 °C. Then, the tubes were centrifuged for 10 min at a speed of 4000 rpm. The resulting supernatant was filtered through a 0.45 μm membrane. The absorbance of the supernatant at the wavelength of 665 nm was measured using a spectrophotometer.

2.4.5. Data Analysis

The amount of MB adsorbed by biochar was calculated using Equation (1).

$$q_t = (C_0 - C_t)V/m \quad (1)$$

In Equation (1) q_t (mg g^{-1}) is the adsorption capacity of MB at time t, C_0 (mg·L^{-1}) is the initial MB concentration, and C_t (mg·L^{-1}) is the equilibrium concentration of MB at time t. V is the volume of dye solution, L. The m is the weight of adsorbent used, g.

The kinetic adsorption data were described (fitted) using a pseudo-first-order model and a pseudo-second-order model.

The pseudo-first-order model [25] is described by Equation (2):

$$\ln(q_e - q_t) = \ln(q_e) - k_1 t \quad (2)$$

and the pseudo-second-order model [26] is described by Equation (3):

$$q_t = k_2 \cdot q_e^2 t/(1 + k_2 q_e^2 t) \quad (3)$$

In Equations (2) and (3), q_t and q_e (mg g^{-1}) are the adsorption capacity of MB on biochar at time t and at equilibrium time, respectively; and k_1 (min^{-1}) and k_2 (g mg^{-1} min^{-1}) are the rate constants of the pseudo-first-order and pseudo-second-order kinetic reactions, respectively.

The adsorption isotherm data were fitted using the Langmuir and Freundlich models.

The Langmuir model [27] is described by Equation (4):

$$q_e = q_m K_L C_e/(1 + K_L C_e) \quad (4)$$

The Freundlich model [28] is described by Equation (5):

$$q_e = K_f C_e^{1/n} \quad (5)$$

In Equations (4) and (5), C_e (mg L^{-1}) is the equilibrium concentration of the solution; q_e (mg g^{-1}) is the equilibrium adsorption capacity; K_L is a constant for the Langmuir model; q_m (mg g^{-1}) is the maximum adsorption capacity; K_f (L mg^{-1}) is a constant for the Freundlich model; and 1/n is the adsorption affinity constant.

3. Results and Discussion

3.1. Characterization of Biochars

The scanning electron microscopy (SEM) micrographs of CSBC, KOH-CSBC and H_3PO_4-CSBC are shown in Figure 1. The morphology of corn stalk remained in the CSBC. Some fragments that appeared in the CSBC were mainly from the thermal decomposition of cellulose and hemicelluloses. The pyrolysis temperature for CSBC was 500 °C. Thermal decomposition of cellulose, hemicellulose and lignin occurs at 220–315 °C, 315–400 °C and 160–900 °C, respectively [29]. After KOH modification, the biochar pore structure became more developed, and more fragments were observed on the surface of the KOH-CSBC. Some crystal particles also appeared on the surface of KOH-CSBC. The mineral components were formed from the thermal decomposition of KOH. Meanwhile, the modification of CSBC by KOH promoted the formation of a more microporous structure. The modification of biochar

using H_3PO_4 resulted in different characteristics than those resulting from KOH modification. More fragments in biochar bonded together after H_3PO_4 modification, and the surface of H_3PO_4-modified CSBC exhibited a smooth and gelatinous appearance, and the fragments of CSBC bonded together, inhibiting the formation of a microporous structure.

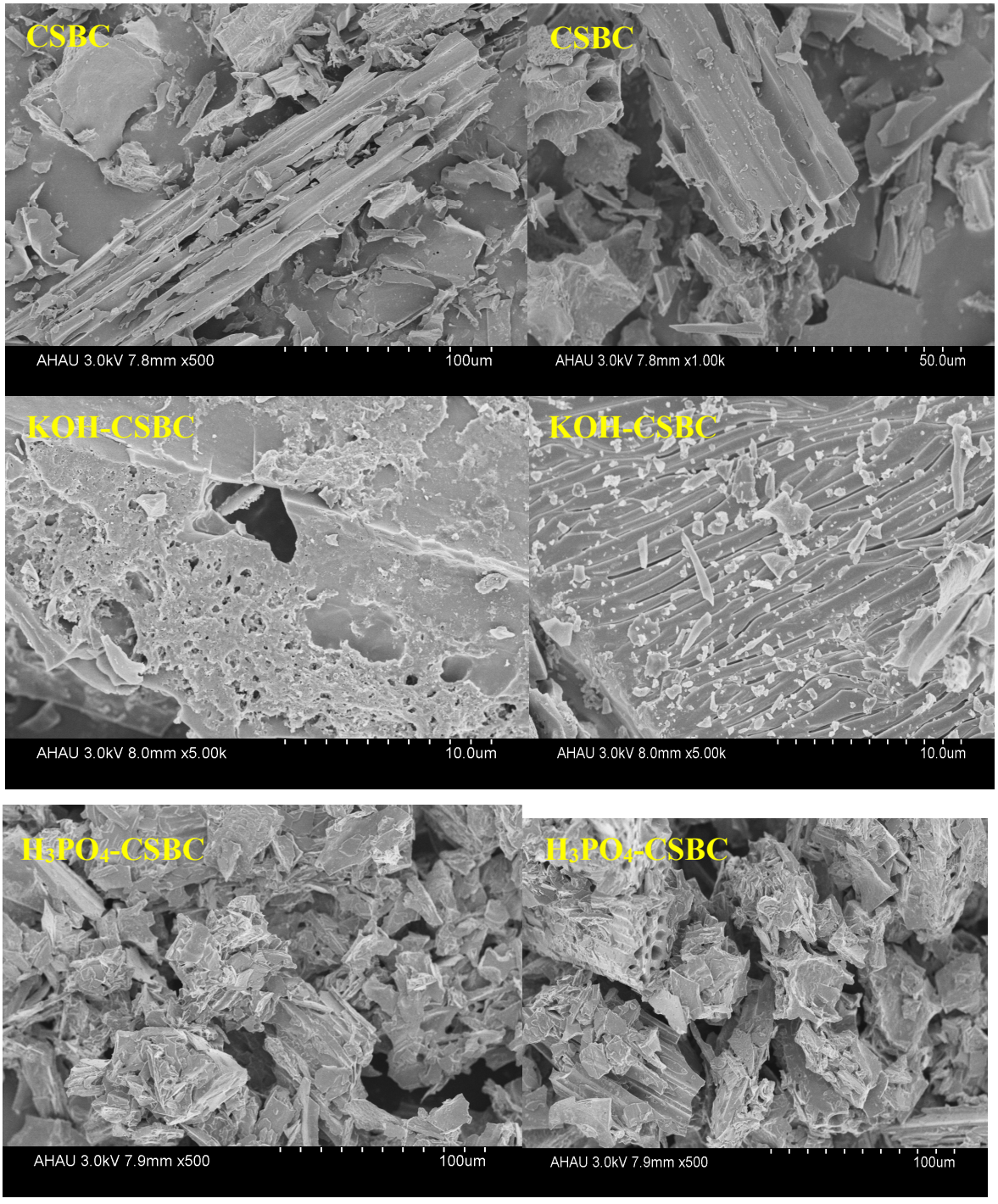

Figure 1. Scanning electron microscope (SEM) micrographs of corn stalk biochar(CSBC), KOH-CSBC and H_3PO_4-CSBC.

The surface area, pore volume and pore size of biochars are displayed in Table 1. After KOH modification, the surface area of biochar significantly increased from 24.2543 to 473.6432 $m^2 \cdot g^{-1}$. The surface area increased approximately 20 times after KOH activation. The pore volume of KOH-CSBC

also increased and pore size decreased. However, after H_3PO_4 modification, the surface area of biochar decreased from 24.2543 to 2.8404 m^2g^{-1}. The pore volume of H_3PO_4-CSBC also decreased and pore size increased. Thus, the measurements of surface area, pore volume and pore size were consistent with the observations of SEM images. KOH modification obviously influenced the surface structure of biochar, which suggested the treatment could affect the removal of MB from the solution.

Table 1. Surface area, pore volume and pore size of biochars.

Samples	Surface Area (m^2 g^{-1})	Pore Volume (cm^3 g^{-1})	Pore Size (Å)
corn stalk biochar (CSBC)	24	0.021	34.0
KOH-CSBC	474	0.24	20.4
H_3PO_4-CSBC	3	0.0025	35.1

Surface area: Brunauer–Emmett–Teller (BET-N_2) method; Total pore volume of pores; Adsorption average pore width.

The XRD spectra of CSBC, KOH-CSBC and H_3PO_4-CSBC are shown in Figure 2. Amorphous carbon peaks were obvious in spectra from the CSBC. Some minerals also were detected in the CSBC, including $CaCO_3$ and KCl. After KOH modification, K and K_2O were observed in the biochar, suggesting that KOH had reacted with the carbonaceous components in CSBC. Only amorphous carbon was detected in H_3PO_4-CSBC, indicating that H_3PO_4 modification mainly affected the organic components of CSBC.

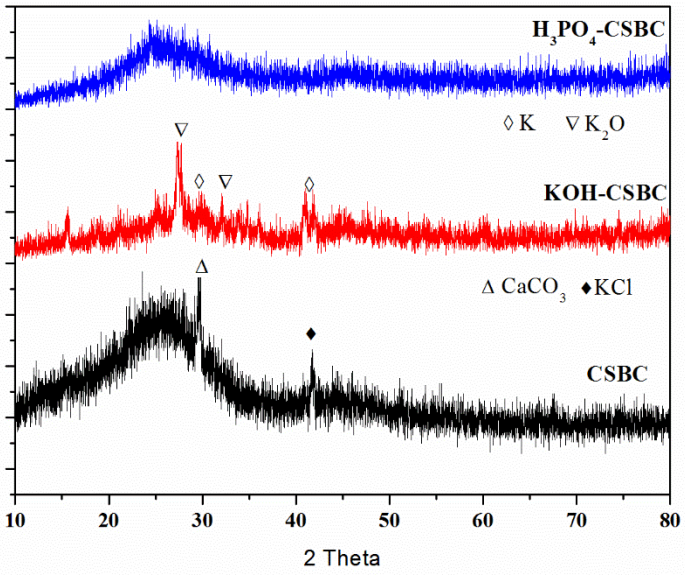

Figure 2. X-ray diffraction (XRD)spectra oftested adsorbents.

The FTIR spectra of CSBC, KOH-CSBC and H_3PO_4-CSBC are presented in Figure 3. The functional groups of CSBC, KOH-CSBC and H_3PO_4-CSBC differed significantly. The specific functional groups for the different types of biochar are shown in Table 2. The main groups in CSBC included OH, aliphatic C, C=O and C=C, carboxyl anions (affected by C=O stretching), Si–O and C–H [30]. The main groups in KOH-CSBC included OH, C=O and C=C, substances in the phenolic O–H band, alkenes (affected by C–H bending), cellulosic ethers (affected by C–O–C stretching), aromatic C–H, and CH–of alkenes and alkane [31]. The modification of KOH led to the disappearance of aliphatic C and carboxyl anions due to the high pyrolytic temperature (700 °C). The appearance of the phenolic O–H band, C–H bending of alkenes, and C–O–C stretching indicated the formation of olefin compounds. The existence of aromatic C–Hand aromatic C–O stretching suggested the further enhancement of the CSBC's aromatic structure.

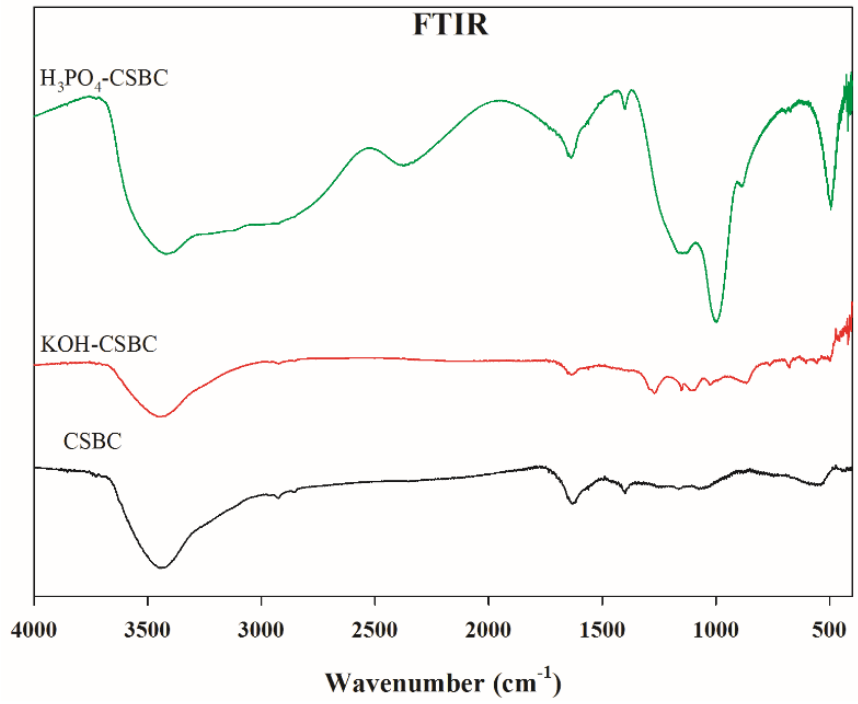

Figure 3. Fourier transform infrared (FTIR) spectra of tested adsorbents.

Table 2. The main functional groups of CSBC, KOH-CSBC and H_3PO_4-CSBC.

CSBC		KOH-CSBC		H_3PO_4-CSBC	
Wavenumber (cm^{-1})	**Assignment**	**Wavenumber (cm^{-1})**	**Assignment**	**Wavenumber (cm^{-1})**	**Assignment**
3443	–OH	3450	–OH	3425	–OH
2925	aliphatic C			2372	C–O vibrations
1633	C=O and C=C	1637	C=O and C=C	1637	C=O and C=C
1560	C=O stretching	1271	aromatic C–O stretching	1401	–COOH or O–H bending
1075	Si–O stretching vibrations	1151	phenolic O–H band	1145	amino phosphonic acid functional group
539	aromatic C–H stretching	1103	C–H bending of alkenes	998	P–OH bond
		1025	C–O–C stretch	495	Si–O–Si
		867	Aromatic C–H		
		676	CH–of alkenes and alkanes		

The functional groups in H_3PO_4-CSBC included–OH, substances exhibiting C–O vibration, C=O and C=C, –COOH, substances exhibiting O–H bending deformation, amino phosphonic acid functional group, P–OH bonded substances and Si–O–Si [20–22]. The modification of H_3PO_4 caused the disappearance of aliphatic C and carboxyl anions owing to the high pyrolytic temperature (700 °C). Meanwhile, the observation of C–O, –COOH and O–H bending deformation illustrated the enhancement of the CSBC's aromatic structure. Furthermore, the presence of the amino phosphonic acid functional group and P-OH bonds in H_3PO_4-CSBC demonstrated that a reaction happened between H_3PO_4 and the carbonaceous components in biochar. The introduction of phosphorous-containing functional groups on biochar may play an important role for MB removal.

The XPS spectra of CSBC, KOH-CSBC and H_3PO_4-CSBC are shown in Figure 4. C, O, N and P were detected in all biochars, but C and O were dominant. The relative content of P increased and the relative content of N decreased after KOH modification. The relative content of C decreased and the relative content of O and P decreased after H_3PO_4 modification.

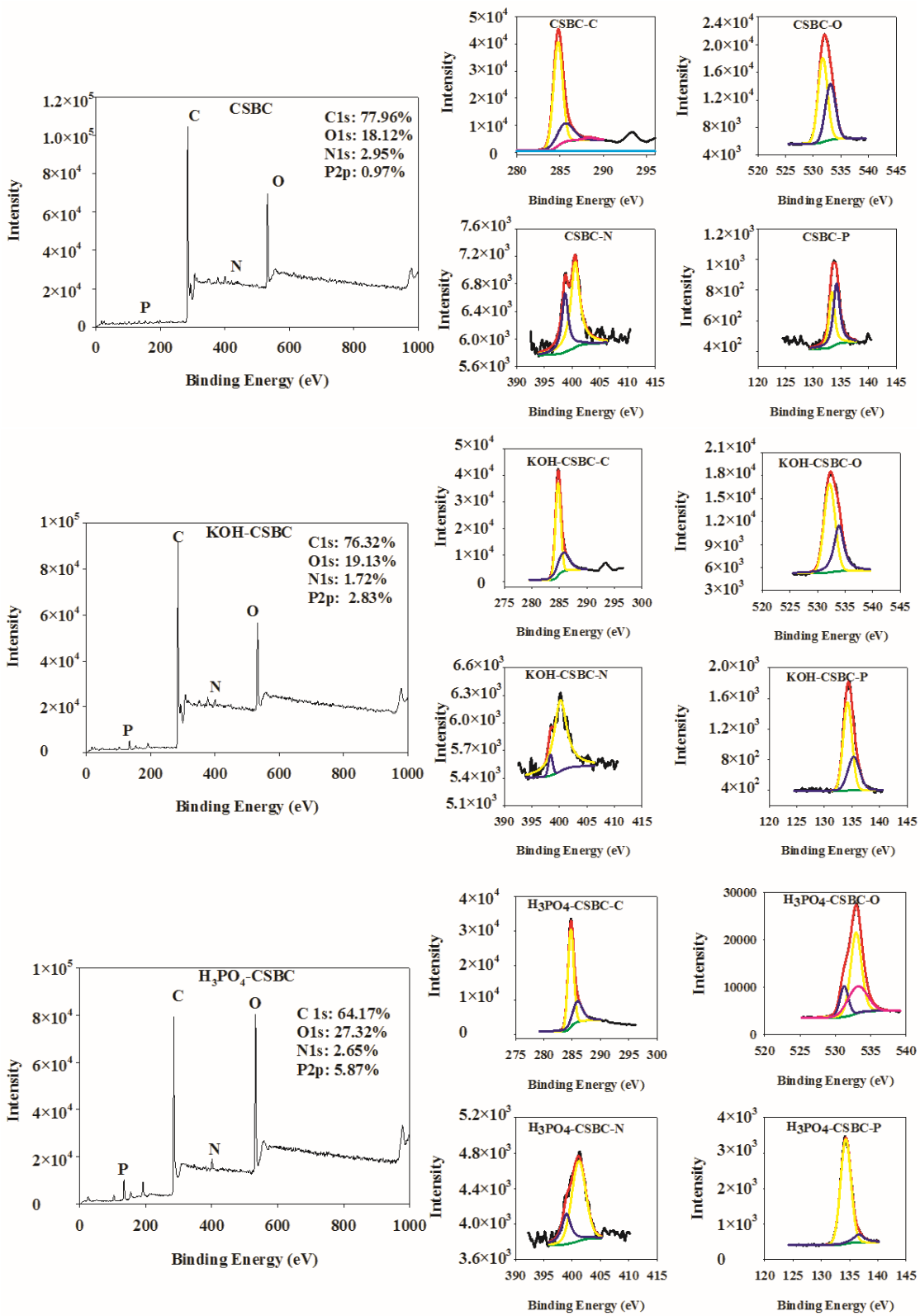

Figure 4. X-ray photoelectron spectroscopy (XPS) spectra of tested adsorbents.

Results from the XPS peak-differentiating analysis for CSBC, KOH-CSBC and H_3PO_4-CSBC are displayed in Table 3. The C-1s XPS spectra of biochar exhibited three peaks at 284.77, 285.58 and 288.34 eV, corresponding to the carbon-based functional groups C–C/C–H, C–O and O=C–O, respectively [32–34]. The carbon functional groups in CSBC included C–C/C–H, C–O and O=C–O.

The carbon-based functional groups in KOH-CSBC and H_3PO_4-CSBC included C–C/C–H and C–O. The O=C–O functional group could not be detected in either KOH-CSBC or H_3PO_4-CSBC due to the thermal decomposition of carbonaceous components. The relative content of C-C/C-H decreased and the relative content of C-O increased in both KOH-CSBC and H_3PO_4-CSBC on account of the introduction of the activating agents.

Table 3. Functional groups and peak fitting of tested adsorbents based on XPS studies.

Functional Groups		CSBC	KOH-CSBC	H_3PO_4-CSBC
C	C–C/C–H	284.77 [a] 72.55% [b]	284.78 66.57%	284.78 68.70%
	C–O	285.58 24.23%	285.74 33.43%	286.07 31.30%
	O=C–O	288.34 3.22%		
O	C–O	531.73 58.23%	532.19 61.00%	531.23 (C=O/O=P) 15.77%
	C=O–OH	533.12 41.77%	533.88 39.00%	533.10 30.19%
	O–C/COH/C–O–C/P-O			532.91 54.04%
N	Pyrimidine nitrogen	398.72 33.39%	398.41 6.27%	398.99 25.83%
	Pyrrole nitrogen/ pyridine nitrogen	400.57 66.61%	400.19 93.73%	401.16 74.17%
P	$C–PO_3/C_2–PO_2$	133.38 41.90%		
	$C–O–PO_3$	134.22 58.10%	134.23 65.48%	134.33 88.94%
	P_2O_5		135.33 34.52%	136.60 11.06%

[a] Binding energy, eV; [b] The relative percentage of functional groups, %.

The O-1s XPS spectra of pristine biochar exhibited three peaks at 531.73, 533.12 and 532.91 eV, corresponding to C–O, C=O–OH and C=O/O=P/O–C/COH/C–O-C/P–O, respectively [35,36]. The oxygen-based functional groups included C–O and C=O–OH in CSBC. The main oxygen-based functional groups were C–O and C=O–OH in KOH-CSBC. The group C=O/O=P O–C/C–OH/C–O–C/P–O was observed in biochar after H_3PO_4 modification. Thus, H_3PO_4 modification obviously affected the types and relative content of oxygen-containing groups, indicating that this change could influence the removal of MB from solution.

The N-1s XPS spectra of biochar exhibited two peaks at 398.72 eV and 400.57 eV, corresponding to pyrimidine and pyridine/pyrrole, respectively [37]. The main nitrogen-containing groups were pyrimidine and pyridine/pyrrole in CSBC. The main group was pyridine/pyrrole in KOH-CSBC. The relative content of pyrimidine decreased after KOH modification. The relative content of pyridine/pyrrole increased slightly after H_3PO_4 modification.

The P-2p XPS spectra of biochar exhibited three peaks at 133.38 eV, 134.22 eV and 135.33 eV corresponding to C-PO_3/C_2-PO_2, C-O-PO_3 and P_2O_5, respectively [38–41]. The phosphorous-based functional groups were C–PO_3/C_2–PO_2 and C–O–PO_3 in CSBC. After KOH modification, C–O–PO_3 and P_2O_5 were the main phosphorus-containing groups in KOH-CSBC. Meanwhile, C–O–PO_3 was the dominant phosphorous-containing group in H_3PO_4-CSBC. P_2O_5 also was found in H_3PO_4-CSBC. The XPS analysis confirmed that H_3PO_4 reacted with the carbonaceous components in biochar and that

H_3PO_4 itself occurred in thermal decomposition. H_3PO_4 modification enriched the functional groups in biochar, indicating that more binding sites would be available to remove MB from solution.

3.2. Effect of Solid-to-Liquid Ratio and Initial pHon MB Removal

The effect of solid-to-liquid ratio on MB removal by CSBC, KOH-CSBC and H_3PO_4-CSBC is shown in Figure 5a. When the solid-to-liquid ratio increased from 0.5 g L^{-1} to 4 g L^{-1}, the efficiency of removing MB by CSBC, KOH-CSBC and H_3PO_4-CSBC increased from 13% to 59%, from 99.6% to 100%, and from 93% to 100%, respectively. Higher solid–liquid ratio means a larger amount of adsorbent and a larger number of binding sites for the removal of MB. Compared with pristine biochar (CSBC), the biochar modified by KOH and H_3PO_4 significantly increased the removal of MB at any given solid-to-liquid ratio. Thus, the modification of biochar using these two activation agents was effective. The efficiency of removing MB by KOH-CSBC and H_3PO_4-CSBC was nearly 100% when the solid-to-liquid ratio was equivalent to 1.0 g L^{-1}.

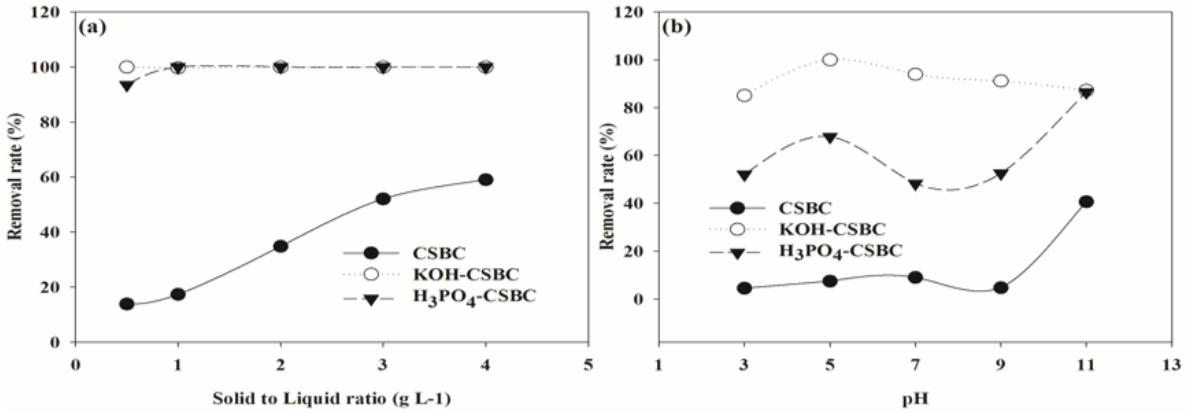

Figure 5. Effect of (**a**) Solid to Liquid ratio and (**b**) pH on methylene blue (MB) removal.

The effect of initial pH on MB removal by CSBC, KOH-CSBC and H_3PO_4-CSBC is shown in Figure 5b. The efficiency of removing MB by CSBC, KOH-CSBC and H_3PO_4-CSBC was 41%, 87% and 86% at pH 11.0, respectively. However, the maximum MB removal efficiency achieved by KOH-CSBC was nearly 100% at pH 5.0.

As pH increased, the efficiency of removing MB by CSBC first increased and then tended to stabilize. The removal of MB by CSBC was more favorable under alkaline conditions because MB is a cationic dye. The removal of MB by KOH-CSBC as pH increased first increased and then slightly decreased. The overall removal rate was more than 85% at pH 3.0–11.0. The reduced MB removal rate of KOH-CSBC at higher pH (7.0–11.0) may be related to the loss of binding sites under alkaline conditions. The efficiency of removing MB by H_3PO_4-CSBC at pH first increased, then slightly decreased and finally exhibited a slight increase. These changes in removal efficiency may have been caused by the protonation or deprotonation of phosphorus-containing groups in H_3PO_4-CSBC at different pH [42].

3.3. Adsorption Kinetics of MB on Biochars

The adsorption kinetics of MB and theoretical fitted curves for CSBC, KOH-CSBC and H_3PO_4-CSBC are presented in Figure 6. As reaction time increased, the amount of MB adsorbed on CSBC, KOH-CSBC and H_3PO_4-CSBC first increased quickly and then tended to stabilize. Thus, the adsorption process could be divided into a fast stage and a slow stage. In the initial phase of adsorption (fast stage), the MB molecules rapidly occupied the vacant sites on the surface of biochar. After 30 min (i.e., the end of the fast stage and beginning of the slow stage), the decreased number of vacant adsorption sites on the surface of biochar led to the saturation of adsorption capacity. The adsorption process gradually reached equilibrium after approximately 60 min.

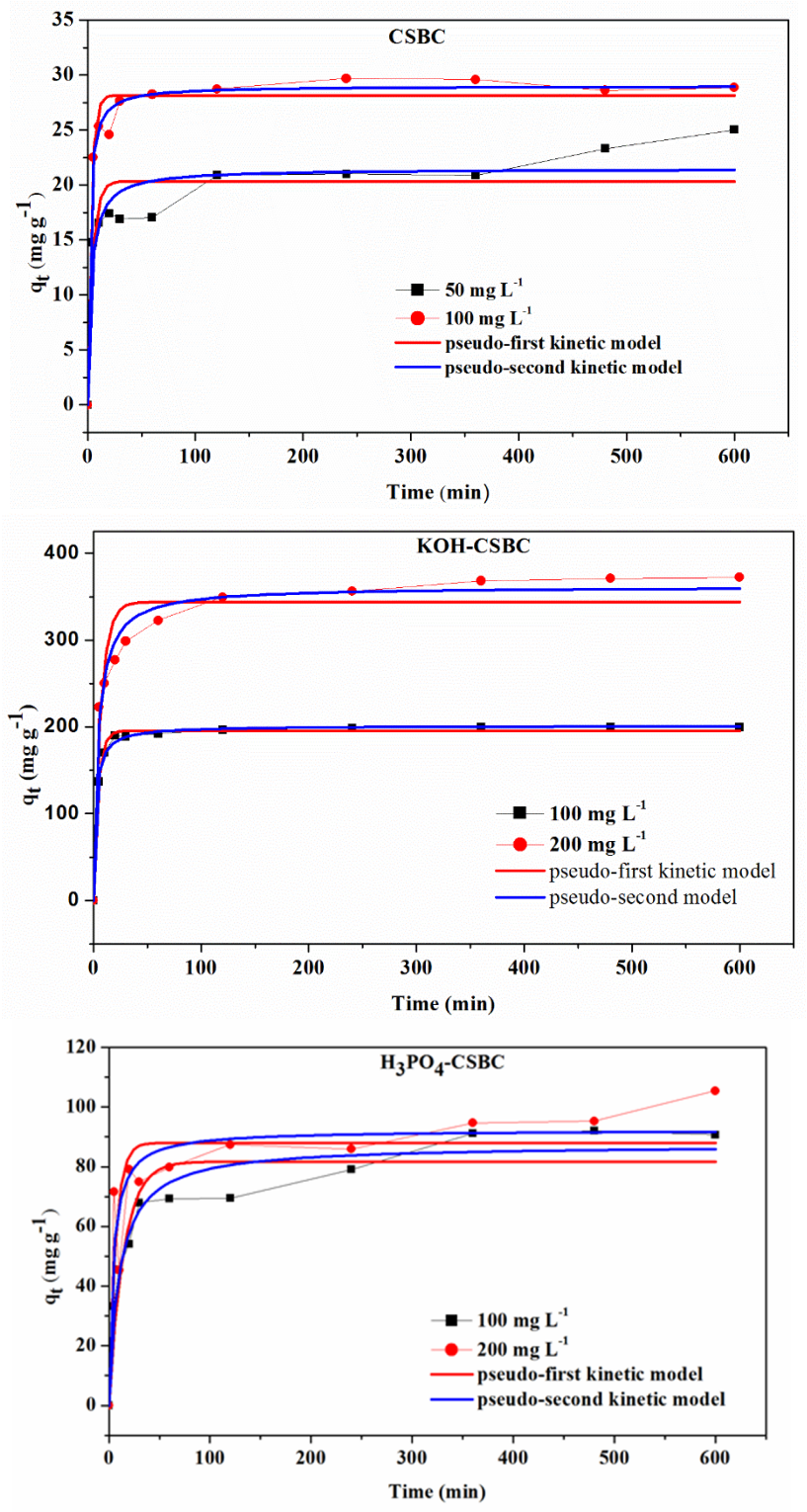

Figure 6. Adsorption kinetics and theoretical fitting curves of MB on tested adsorbents.

The amount of MB adsorbed from the more highly concentrated solution by biochars was larger than that adsorbed from the less highly concentrated solution. When the concentration of MB increased from 50 mg L^{-1} to 100 mg L^{-1}, the amount of MB adsorbed on CSBC increased from 25.0 mg g^{-1} to 28.8 mgg^{-1}. Likewise, when the concentration of MB increased from 100 mg L^{-1} to 200 mg L^{-1}, the amount of MB adsorbed on KOH-CSBC and H_3PO_4-CSBC increased from 199.8 to 372.3 mg g^{-1}, and from 91 to 105 mg g^{-1}, respectively. A higher initial concentration of MB can provide a higher driving

force to overcome the mass transfer resistance of dye molecules between the solid phase and the liquid phase, resulting in more contact between dye molecules and the active sites on an adsorbent [43,44]. This phenomenon likely explains the data shown in Figure 6.

The parameters used to model the adsorption kinetics of MB on CSBC, KOH-CSBC and H_3PO_4-CSBC are shown in Table 4. Compared with predictions using the pseudo-first-order model, the pseudo-second-order model provided a better description of the MB adsorption process, suggesting the adsorption of MB molecules on biochars contained multiple steps (including external liquid film diffusion, surface adsorption and particle diffusion) [45]. Furthermore, chemical interaction played an important role during the MB adsorption process [46].

Table 4. Pseudo-first-order and pseudo-second-order kinetic models adsorption parameters.

Samples	Pseudo-First-Order			Pseudo-Second-Order		
	k_1 (min^{-1})	q_e (mg g^{-1})	R^2	k_2 (g mg^{-1}·min^{-1})	q_e (mg g^{-1})	R^2
CSBC-50	0.21345	20.32061	0.83583	0.01439	21.47248	0.90152
CSBC-100	0.29512	28.16607	0.96912	0.02148	29.00599	0.98949
KOH-CSBC-100	0.22694	195.77074	0.99472	0.00238	201.40582	0.99655
KOH-CSBC-200	0.14885	343.79494	0.91663	6.55037×10^{-4}	361.7548	0.97949
H_3PO_4-CSBC-100	0.06862	81.7322	0.89829	0.00112	87.36304	0.95485
H_3PO_4-CSBC-200	0.14954	87.97926	0.76541	0.00273	92.28821	0.84763

3.4. Adsorption Isotherms

The adsorption isotherms and fitted prediction curves describing adsorption of MB on CSBC, KOH-CSBC and H_3PO_4-CSBC are displayed in Figure 7. As the MB concentration increased, the amount of MB adsorbed on CSBC, KOH-CSBC and H_3PO_4-CSBC first increased and then tended to stabilize. A higher initial MB concentration resulted in higher adsorption, which followed the order KOH-CSBC>H_3PO_4-CSBC>CSBC.

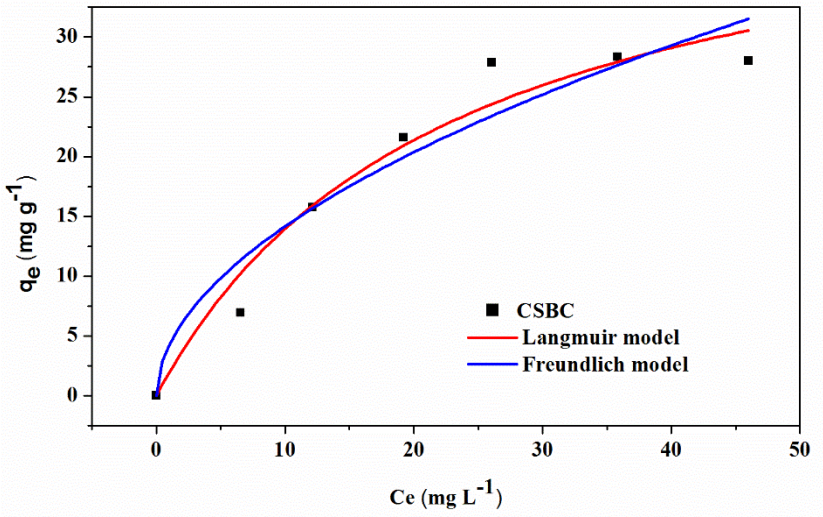

Figure 7. *Cont.*

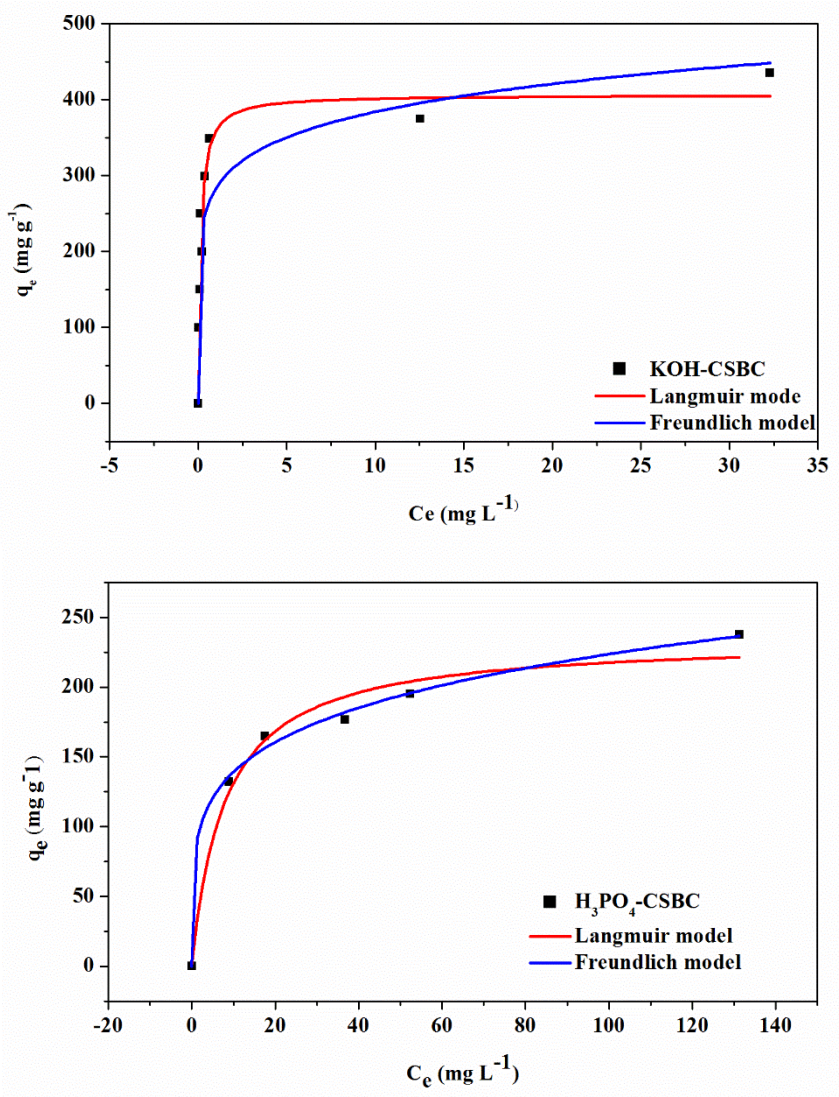

Figure 7. Adsorptionisotherm and fitting curves of MB on tested adsorbents.

The parameters used to model the adsorption isotherm of MB on CSBC, KOH-CSBC, H_3PO_4-CSBC are shown in Table 5. Both the Langmuir and Freundlich models described the adsorption process of MB on biochars well, as indicated by correlation coefficients that exceeded 0.85. The Langmuir isotherm better fit the adsorption process of MB on CSBC and KOH-CSBC (with correlation coefficients in the range 0.87–0.95). Technically, the Freundlich model described the adsorption process of MB on H_3PO_4-CSBC better, exhibiting a correlation coefficient of 0.99 compared to that (0.97) for the Langmuir model.

Table 5. Fitting parameters of adsorption isotherms.

Samples	Langmuir			Freundlich		
	q_m(mg·g^{-1})	K_L (L·mg^{-1})	R^2	K_F	1/n	R^2
CSBC	45.58	0.04415	0.9535	4.232	0.5245	0.9145
KOH-CSBC	406.43	7.553	0.9084	283.21	0.1321	0.8665
H_3PO_4-CSBC	234.75	0.1267	0.9746	86.67	0.2058	0.9955

Based on the fitted Langmuir model, the maximum adsorption capacity of CSBC, KOH-CSBC and H_3PO_4-CSBC for MB was 45.58 mg·g^{-1}, 406.43 mg·g^{-1} and 234.75 mg g^{-1}, respectively. The adsorption

capacities of KOH-CSBC and H_3PO_4-CSBC were 9.4 and 5.3 times higher than CSBC, respectively. Thus, KOH and H_3PO_4 modification significantly enhanced the adsorption capacity of biochar for MB, with KOH modification producing nearly twice the increase achieved by H_3PO_4.

The parameter K_L (Equation (4)) reflected the adsorption affinity between biochar and MB molecules [47]. In this study, the K_L associated with KOH-CSBC was larger than that for both H_3PO_4-CSBC and CSBC, indicating that KOH-CSBC had a higher affinity for MB than CSBC and H_3PO_4-CSBC. Similarly, the parameter 1/n derived for the Freundlich model reflected the difficulty of MB adsorption. Generally, when 1/n is less than 0.5, an adsorbent is easily adsorbed, and when 1/n exceeds 2, the adsorbent is hardly adsorbed [48]. In this research, the value of 1/n for KOH-CSBC and H_3PO_4-CSBC was less than 0.5, suggesting the adsorption of MB proceeded easily. Meanwhile, the value of 1/n for CSCB was 0.52448, illustrating that adsorption MB could occur, albeit with slightly more difficulty than for KOH-CSBC and H_3PO_4-CSBC.

3.5. Discussion of Activation Mechanism and Adsorption Mechanism

3.5.1. Activation Mechanism

In this study, modification (activation) of corn stalk biochar using KOH and H_3PO_4 greatly improved the removal of MB from solution.

KOH activation was an effective method through which to create a porous structure in biochar. Previous studies [49–53] found that the activation mechanism of KOH is as follows. First, KOH melted at 360 °C and then was involved in a reduction reaction with carbon precursors that formed K_2CO_3 at nearly 400 °C. KOH was gradually consumed at 600 °C and converted entirely to K_2CO_3. K_2CO_3 decomposed into CO_2 and K_2O when the temperature exceeded 700 °C and disappeared completely at 800°C. Additionally, the generated CO_2 reacted with other sources of C to form CO at high temperature. Meanwhile, potassium compounds were reduced to metallic potassium by carbon at high temperatures. When the alkaline metal became a highly diffused vapor, it was easily inserted into the carbon lattice and thus generated a more well-developed porous structure in the biochar. The reaction process is described in Equations (6)–(10).

The influence of KOH activation on CSBC was easily observed through surface area analysis and by SEM, XRD, FTIR and XPS characterization. Based on surface area measurements and SEM images, the biochar exhibited a larger surface area and better developed pore structure after KOH modification. XRD analysis detected the existence of K and K_2O. FTIR and XPS analysis confirmed that biochar had a more developed aromatic structure after KOH high-temperature activation. The structural characteristic of KOH-CSCB resulted in a high ability to remove MB from aqueous solution.

$$6KOH + 2C \rightarrow 2K + 2H_2 + 2K_2CO_3 \quad (6)$$

$$K_2CO_3 \rightarrow K_2O + CO_2 \quad (7)$$

$$CO_2 + C \rightarrow 2CO \quad (8)$$

$$K_2CO_3 + C \rightarrow 2K + 3CO \quad (9)$$

$$K_2O + C \rightarrow 2K + CO \quad (10)$$

The function of H_3PO_4 is to first act as an acid catalyst to promote bond-cracking reactions. A chain structure is formed by the reaction of ring and condensation in biochar. Second, the reaction with organic components forms phosphate and polyphosphate bridged and crosslinked biopolymer fragments, which promote the formation of pores [41]. As reported in the literature [41,54], H_3PO_4 activation

proceeded as follows. First, in the pyrolysis process, the oxygen-containing functional group of biochar reacted with H_3PO_4 to generate water vapor, which further reacted with the carbonaceous components in biochar to form the inner pore structure, as indicated in the following reaction (Equation (11)).

$$4H_3PO_4 + 10C \rightarrow P_4 + 10CO + 6H_2O \quad (11)$$

Second, the catalysis of H_3PO_4 led to the oxidation and fixation of oxygen-containing functional groups on the pore walls, which led to the reduction of pore size or the transformation of mesopores into micropores. Third, H_3PO_4 promoted the formation of –COOH, –OH, C=C and an aromatic structure, and enhanced the formation of P-O or P-OOH functional groups.

H_3PO_4 modification of biochar promoted the formation of phosphorus-containing functional groups, –COOH, –OH and a highly aromatic structure, as confirmed by FTIR and XPS analysis. However, surface area and pore analyses showed that H_3PO_4 modification did not facilitate the formation of a porous structure of biochar, but instead reduced the specific surface area and pore volume. According to SEM images, the pore structure of biochar was agglomerated and fused, an effect that may be related to the material composition, pyrolysis preparation conditions, or the activation process of H_3PO_4. Mandal et al. [55] showed that the H_3PO_4 treatment of rice straw biochar reduced both surface area and pore volume, and concluded these changes might be due to the increase in functional groups inside the pores following H_3PO_4 treatment. Consequently, the improvement of MB adsorption capacity by H_3PO_4 treatment of CSBC was independent of the specific surface area and pore structure; rather, other mechanisms determined the high MB adsorption capacity of H_3PO_4-CSBC. FTIR and XPS analyses showed that H_3PO_4 modification obviously affected the oxygen- and phosphorus-containing functional groups of biochar. Torrellas et al. also found that more functional groups existed on the activated carbon after H_3PO_4 activation [56]. The participation of these functional groups was an important reason for the high MB adsorption capacity of H_3PO_4-CSBC.

3.5.2. Removal Mechanism of Methylene Blue by Biochar

The main mechanisms for MB removal by adsorbent or biochar involve physical interaction, ion exchange, electrostatic interaction, π–π stacking, hydrogen bonding and pore filling [48,57–65]. The dominant mechanisms depend on the physicochemical properties of biochar and specific environmental conditions in the solution.

In this study, corn stalk biochar was prepared at 500 °C. Cellulose and hemicellulose in the corn stalk gradually decomposed thermally at temperatures less than 500 °C. Meanwhile, the carbohydrate, protein and fat compounds also gradually decomposed. Then, the specific surface area became larger and a pore structure gradually formed, both of which would play an important role in MB removal. Furthermore, the aromatic structure of the biochar was gradually improved. The aromatic structure of the biochar could combine with the benzene ring in MB molecules via π–π stacking. CSBC contained abundant functional groups among which –OH and –COOH could bind with nitrogen molecules in MB through hydrogen bonding. The pH experiment indicated that electrostatic interaction also could affect the combination between CSBC and MB. Therefore, the adsorption mechanism between CSBC and MB was the result of electrostatic interaction, hydrogen bonding, π–π stacking and physical interaction (surface contact and pore diffusion).

After KOH modification, the surface area and pore volume of biochar significantly increased. The capacity of KOH-CSBC to absorb MB was greatly increased compared to that of pristine CSBC. Thus, the specific surface area and pore volume of KOH-CSBC played a key role in MB adsorption. The variety of functional groups in KOH-CSBC was limited, especially for oxygen-containing groups. Organic groups in KOH-CSBC disappeared at the pyrolytic temperature of 700 °C, resulting in weak hydrogen bonds and weak electrostatic interaction between KOH-CSBC and MB. However, the aromatic structure and the degree of graphitization of KOH-CSBC became stronger compared to pristine CSBC, and the contribution of π–π stacking to MB removal was relatively more important. Therefore, the main MB

removal mechanism of KOH-CSBC involved π–π stacking and physical interaction (surface area and pore diffusion).

After H_3PO_4 modification, the surface area and pore volume of biochar decreased relative to that of pristine CSBC. However, the capacity of H_3PO_4-CSBC to adsorb MB apparently increased, indicating that surface area and pore volume did not play a major role in MB removal by this biochar. FITR analysis showed that H_3PO_4-CSBC contained abundant functional groups, including -OH, -COOH, amino phosphonic acid functional group, and P-OH bond. Hydrogen bonding and electrostatic interaction were critical for MB removal by H_3PO_4-CSBC. Meanwhile, the aromatic structure and the graphitization degree of biochar were enhanced after H_3PO_4 modification. Thus, the main MB removal mechanism of H_3PO_4-CSBC included electrostatic interaction, hydrogen bonding, and π–π stacking.

The MB removal mechanisms by CSBC, KOH-CSBC and H_3PO_4-CSBC are summarized in Figure 8.

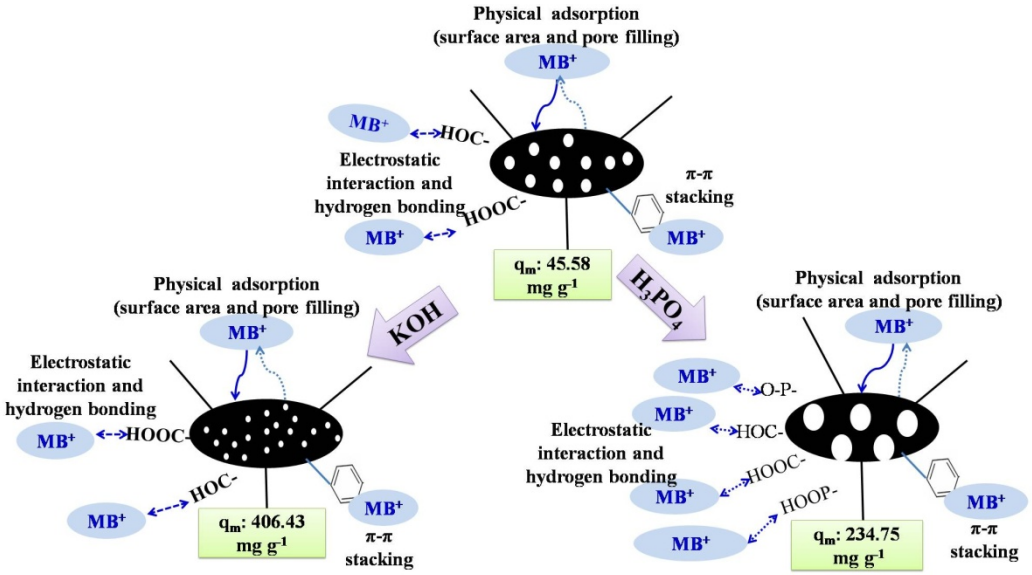

Figure 8. Schematic diagram of removal mechanism between CSBC, KOH-CSBC, H_3PO_4-CSBC and MB.

4. Conclusions

Biochar was prepared from corn stalk and was modified using KOH and H_3PO_4. KOH modification of corn stalk biochar significantly increases the surface area and pore volume of the biochar. H_3PO_4 modification enriches the functional groups of biochar. As a result of both types of biochar modification, the maximum adsorption capacity for MB increases approximately 5–10 times (in this study from 43.14 mg g^{-1} for CSBC to 406.43 mg g^{-1} for KOH-CSBC and to 230.39 mg g^{-1} for H_3PO_4-CSBC). The modification of corn stalk biochar by KOH and H_3PO_4 also affects the MB adsorption mechanism. Therefore, corn stalk is an ideal natural raw material for preparation of biochar, and biochar production represents an effective way to utilize corn residues. Corn stalk biochar, especially if modified by KOH or to a lesser extent by H_3PO_4, can be applied to remove MB-based dye from wastewater.

Author Contributions: Conceptualization and methodology, L.L. and S.F.; writing—original draft preparation, L.L. and S.F.; writing—review and editing, L.L., Y.L. and S.F.; supervision, Y.L. and S.F.

Funding: This study was funded by National Natural Science Foundation of China, grant number 51809001; Natural Science Foundation of the Education Department of Anhui Province, grant number KJ2018A0125, KJ2018A0347; Fuyang Normal University Youth Fund Project, grant number No. 204008134, 2018FSKJ07ZD.

Conflicts of Interest: The authors have declared no conflict of interest.

Statement of Novelty: KOH and H_3PO_4 were used to modify corn stalk biochar. The order of adsorption capacity was KOH-CSBC>H_3PO_4-CSBC>CSBC.The interaction mechanism between biochars and methylene blue were different.

References

1. Rajoriya, S.; Bargole, S.; George, S.; Saharan, V.K. Treatment of textile dyeing industry effluent using hydrodynamic cavitation in combination with advanced oxidation reagents. *J. Hazard. Mater.* **2018**, *344*, 1109–1115. [CrossRef] [PubMed]
2. Hui, M.; Shengyan, P.; Yaqi, H.; Rongxin, Z.; Anatoly, Z.; Wei, C. A highly efficient magnetic chitosan "fluid" adsorbent with a high capacity and fast adsorption kinetics for dyeing wastewater purification. *Chem. Eng. J.* **2018**, *345*, 556–565. [CrossRef]
3. Lehmann, J.; Rillig, M.C.; Thies, J.; Masiello, C.A.; Hockaday, W.C.; Crowley, D. Biochar effects on soil biota—A review. *Soil Biol. Biochem.* **2011**, *43*, 1812–1836. [CrossRef]
4. Xiao, X.; Chen, B.; Chen, Z.; Zhu, L.; Schnoor, J.L. Insight into Multiple and Multilevel Structures of Biochars and Their Potential Environmental Applications: A Critical Review. *Environ. Sci. Technol.* **2018**, *52*, 5027–5047. [CrossRef] [PubMed]
5. Ahmad, M.; Rajapaksha, A.U.; Lim, J.E.; Zhang, M.; Bolan, N.; Mohan, D.; Vithanage, M.; Lee, S.S.; Ok, Y.S. Biochar as a sorbent for contaminant management in soil and water: A review. *Chemosphere* **2014**, *99*, 19–33. [CrossRef] [PubMed]
6. Gao, B.; Yao, Y.; Xue, Y.; Zimmerman, A.; Mosa, A.; Pullammanappallil, P.; Ok, Y.S.; Cao, X. A review of biochar as a low-cost adsorbent for aqueous heavy metal removal AU—Inyang, Mandu I. *Crit. Rev. Environ. Sci. Technol.* **2016**, *46*, 406–433.
7. Mohan, D.; Sarswat, A.; Ok, Y.S.; Pittman, C.U. Organic and inorganic contaminants removal from water with biochar, a renewable, low cost and sustainable adsorbent—A critical review. *Bioresour. Technol.* **2014**, *160*, 191–202. [CrossRef]
8. Trinh, B.-S.; Le, T.K.P.; Werner, D.; Phuong, H.N.; Luu, L.T. Rice Husk Biochars Modified with Magnetized Iron Oxides and Nano Zero Valent Iron for Decolorization of Dyeing Wastewater. *Processes* **2019**, *7*, 660. [CrossRef]
9. Zhang, Y.; Lou, Z.; Wang, C.; Wang, W.; Cai, J. Synthesis of Porous Fe/C Bio-Char Adsorbent for Rhodamine B from Waste Wood: Characterization, Kinetics and Thermodynamics. *Processes* **2019**, *7*, 150. [CrossRef]
10. Liu, W.-J.; Jiang, H.; Yu, H.-Q. Development of Biochar-Based Functional Materials: Toward a Sustainable Platform Carbon Material. *Chem. Rev.* **2015**, *115*, 12251–12285. [CrossRef]
11. Li, H.; Dong, X.; da Silva, E.B.; de Oliveira, L.M.; Chen, Y.; Ma, L.Q. Mechanisms of metal sorption by biochars: Biochar characteristics and modifications. *Chemosphere* **2017**, *178*, 466–478. [CrossRef] [PubMed]
12. Rajapaksha, A.U.; Chen, S.S.; Tsang, D.C.W.; Zhang, M.; Vithanage, M.; Mandal, S.; Gao, B.; Bolan, N.S.; Ok, Y.S. Engineered/designer biochar for contaminant removal/immobilization from soil and water: Potential and implication of biochar modification. *Chemosphere* **2016**, *148*, 276–291. [CrossRef] [PubMed]
13. Tan, X.-F.; Liu, S.-B.; Liu, Y.-G.; Gu, Y.-L.; Zeng, G.-M.; Hu, X.-J.; Wang, X.; Liu, S.-H.; Jiang, L.-H. Biochar as potential sustainable precursors for activated carbon production: Multiple applications in environmental protection and energy storage. *Bioresour. Technol.* **2017**, *227*, 359–372. [CrossRef] [PubMed]
14. Park, J.; Hung, I.; Gan, Z.; Rojas, O.J.; Lim, K.H.; Park, S. Activated carbon from biochar: Influence of its physicochemical properties on the sorption characteristics of phenanthrene. *Bioresour. Technol.* **2013**, *149*, 383–389. [CrossRef] [PubMed]
15. Dehkhoda, A.M.; Ellis, N.; Gyenge, E. Effect of activated biochar porous structure on the capacitive deionization of NaCl and ZnCl2 solutions. *Microporous Mesoporous Mater.* **2016**, *224*, 217–228. [CrossRef]
16. Liu, D.; Hao, Z.; Zhao, X.; Su, R.; Feng, W.; Li, S.; Jia, B. Effect of Physical and Mechanical Activation on the Physicochemical Structure of Coal-Based Activated Carbons for SO_2 Adsorption. *Processes* **2019**, *7*, 707. [CrossRef]
17. Luo, J.; Li, X.; Ge, C.; Müller, K.; Yu, H.; Huang, P.; Li, J.; Tsang, D.C.W.; Bolan, N.S.; Rinklebe, J. Sorption of norfloxacin, sulfamerazine and oxytetracycline by KOH-modified biochar under single and ternary systems. *Bioresour. Technol.* **2018**, *263*, 385. [CrossRef]
18. Bashir, S.; Zhu, J.; Fu, Q.; Hu, H. Comparing the adsorption mechanism of Cd by rice straw pristine and KOH-modified biochar. *Environ. Sci. Pollut. Res.* **2018**, *25*, 11875–11883. [CrossRef]
19. Huang, H.; Tang, J.; Gao, K.; He, R.; Zhao, H.; Werner, D. Characterization of KOH modified biochars from different pyrolysis temperatures and enhanced adsorption of antibiotics. *RSC Adv.* **2017**, *7*, 14640–14648. [CrossRef]

20. Chen, T.; Luo, L.; Deng, S.; Shi, G.; Zhang, S.; Zhang, Y.; Deng, O.; Wang, L.; Zhang, J.; Wei, L. Sorption of tetracycline on H_3PO_4 modified biochar derived from rice straw and swine manure. *Bioresour. Technol.* **2018**, *267*, 431–437. [CrossRef]
21. Peng, H.; Gao, P.; Chu, G.; Pan, B.; Peng, J.; Xing, B. Enhanced adsorption of Cu(II) and Cd(II) by phosphoric acid-modified biochars. *Environ. Pollut.* **2017**, *229*, 846–853. [CrossRef] [PubMed]
22. Zhao, N.; Zhao, C.; Lv, Y.; Zhang, W.; Du, Y.; Hao, Z.; Zhang, J. Adsorption and coadsorption mechanisms of Cr(VI) and organic contaminants on H_3PO_4 treated biochar. *Chemosphere* **2017**, *186*, 422–429. [CrossRef] [PubMed]
23. Hong, J.; Ren, L.; Hong, J.; Xu, C. Environmental impact assessment of corn straw utilization in China. *J. Clean. Prod.* **2016**, *112*, 1700–1708. [CrossRef]
24. Meng, R.; Chen, T.; Zhang, Y.; Lu, W.; Liu, Y.; Lu, T.; Liu, Y.; Wang, H. Development, modification, and application of low-cost and available biochar derived from corn straw for the removal of vanadium(v) from aqueous solution and real contaminated groundwater. *RSC Adv.* **2018**, *8*, 21480–21494. [CrossRef]
25. Lagergren, S. About the Theory of So-Called Adsorption of Solution Substances. *K. Sven. Vetensk. Handl.* **1898**, *24*, 1–39.
26. Blanchard, G.; Maunaye, M.; Martin, G. Removal of heavy metals from waters by means of natural zeolites. *Water Res.* **1984**, *18*, 1501–1507. [CrossRef]
27. Langmuir, I. The adsorption of gases on plane surfaces of glass, mica and platinum. *J. Am. Chem. Soc.* **1918**, *40*, 1361–1403. [CrossRef]
28. Freundlich, H. Über die adsorption in lösungen. *Z. Phys. Chem.* **1907**, *57*, 385–470. [CrossRef]
29. Yang, H.; Rong, Y.; Chen, H.; Dong, H.L.; Zheng, C. Characteristics of hemicellulose, cellulose and lignin pyrolysis. *Fuel* **2007**, *86*, 1781–1788. [CrossRef]
30. Zhang, G.; Zhang, Q.; Sun, K.; Liu, X.; Zheng, W.; Zhao, Y. Sorption of simazine to corn straw biochars prepared at different pyrolytic temperatures. *Environ. Pollut.* **2011**, *159*, 2594–2601. [CrossRef]
31. Zhu, L.; Zhao, N.; Tong, L.; Lv, Y. Structural and adsorption characteristics of potassium carbonate activated biochar. *RSC Adv.* **2018**, *8*, 21012–21019. [CrossRef]
32. Yang, F.; Sun, L.; Zhang, W.; Zhang, Y. One-pot synthesis of porous carbon foam derived from corn straw: Atrazine adsorption equilibrium and kinetics. *Environ. Sci.* **2017**, *4*, 625–635. [CrossRef]
33. Han, M.; Jiang, K.; Jiao, P.; Ji, Y.; Zhou, J.; Zhuang, W.; Chen, Y.; Liu, D.; Zhu, C.; Chen, X.; et al. Bio-butanol sorption performance on novel porous-carbon adsorbents from corncob prepared via hydrothermal carbonization and post-pyrolysis method. *Sci. Rep.* **2017**, *7*, 11753. [CrossRef] [PubMed]
34. Li, H.; Ye, X.; Geng, Z.; Zhou, H.; Guo, X.; Zhang, Y.; Zhao, H.; Wang, G. The influence of biochar type on long-term stabilization for Cd and Cu in contaminated paddy soils. *J. Hazard. Mater.* **2016**, *304*, 40–48. [CrossRef] [PubMed]
35. Wen, T.; Wang, J.; Yu, S.; Chen, Z.; Hayat, T.; Wang, X. Magnetic Porous Carbonaceous Material Produced from Tea Waste for Efficient Removal of As(V), Cr(VI), Humic Acid, and Dyes. *ACS Sustain. Chem. Eng.* **2017**, *5*, 4371–4380. [CrossRef]
36. Srinivasan, P.; Sarmah, A.K. Characterisation of agricultural waste-derived biochars and their sorption potential for sulfamethoxazole in pasture soil: A spectroscopic investigation. *Sci. Total Environ.* **2015**, *502*, 471–480. [CrossRef]
37. Lian, F.; Cui, G.; Liu, Z.; Duo, L.; Zhang, G.; Xing, B. One-step synthesis of a novel N-doped microporous biochar derived from crop straws with high dye adsorption capacity. *J. Environ. Manag.* **2016**, *176*, 61–68. [CrossRef]
38. Rosas, J.M.; Ruiz-Rosas, R.; Rodríguez-Mirasol, J.; Cordero, T. Kinetic study of the oxidation resistance of phosphorus-containing activated carbons. *Carbon* **2012**, *50*, 1523–1537. [CrossRef]
39. Rosas, J.M.; Bedia, J.; Rodríguez-Mirasol, J.; Cordero, T. HEMP-derived activated carbon fibers by chemical activation with phosphoric acid. *Fuel* **2009**, *88*, 19–26. [CrossRef]
40. Puziy, A.M.; Poddubnaya, O.I.; Ziatdinov, A.M. On the chemical structure of phosphorus compounds in phosphoric acid-activated carbon. *Appl. Surf. Sci.* **2006**, *252*, 8036–8038. [CrossRef]
41. Sun, K.; Huang, Q.; Meng, X.; Chi, Y.; Yan, J. Catalytic Pyrolysis of Waste Polyethylene into Aromatics by H_3PO_4-Activated Carbon. *Energy Fuels* **2018**, *32*, 9772–9781. [CrossRef]
42. Puziy, A.M.; Poddubnaya, O.I.; Martínez-Alonso, A.; Suárez-García, F.; Tascón, J.M.D. Surface chemistry of phosphorus-containing carbons of lignocellulosic origin. *Carbon* **2005**, *43*, 2857–2868. [CrossRef]

43. Lee, L.Y.; Gan, S.; Tan, M.S.Y.; Lim, S.S.; Lee, X.J.; Lam, Y.F. Effective removal of Acid Blue 113 dye using overripe Cucumis sativus peel as an eco-friendly biosorbent from agricultural residue. *J. Clean. Prod.* **2016**, *113*, 194–203. [CrossRef]
44. Alizadeh, B.; Ghorbani, M.; Salehi, M.A. Application of polyrhodanine modified multi-walled carbon nanotubes for high efficiency removal of Pb (II) from aqueous solution. *J. Mol. Liq.* **2016**, *220*, 142–149. [CrossRef]
45. Vadivelan, V.; Kumar, K.V. Equilibrium, kinetics, mechanism, and process design for the sorption of methylene blue onto rice husk. *J. Colloid Interface Sci.* **2005**, *286*, 90–100. [CrossRef]
46. Ho, Y.S.; McKay, G. Pseudo-second order model for sorption processes. *Process. Biochem.* **1999**, *34*, 451–465. [CrossRef]
47. Hu, Q.; Liu, Y.; Feng, C.; Zhang, Z.; Lei, Z.; Shimizu, K. Predicting equilibrium time by adsorption kinetic equations and modifying Langmuir isotherm by fractal-like approach. *J. Mol. Liq.* **2018**, *268*, 728–733. [CrossRef]
48. Shi, L.; Zhang, G.; Wei, D.; Yan, T.; Xue, X.; Shi, S.; Wei, Q. Preparation and utilization of anaerobic granular sludge-based biochar for the adsorption of methylene blue from aqueous solutions. *J. Mol. Liq.* **2014**, *198*, 334–340. [CrossRef]
49. Raymundo-Piñero, E.; Azaïs, P.; Cacciaguerra, T.; Cazorla-Amorós, D.; Linares-Solano, A.; Béguin, F. KOH and NaOH activation mechanisms of multiwalled carbon nanotubes with different structural organisation. *Carbon* **2005**, *43*, 786–795. [CrossRef]
50. Lozano-Castelló, D.; Calo, J.M.; Cazorla-Amorós, D.; Linares-Solano, A. Carbon activation with KOH as explored by temperature programmed techniques, and the effects of hydrogen. *Carbon* **2007**, *45*, 2529–2536. [CrossRef]
51. Zhou, J.; Li, Z.; Xing, W.; Shen, H.; Bi, X.; Zhu, T.; Qiu, Z.; Zhuo, S. A New Approach to Tuning Carbon Ultramicropore Size at Sub-Angstrom Level for Maximizing Specific Capacitance and CO_2 Uptake. *Adv. Funct. Mater.* **2016**, *26*, 7955–7964. [CrossRef]
52. Wang, J.; Kaskel, S. KOH activation of carbon-based materials for energy storage. *J. Mater. Chem.* **2012**, *22*, 23710–23725. [CrossRef]
53. Dehkhoda, A.M.; Gyenge, E.; Ellis, N. A novel method to tailor the porous structure of KOH-activated biochar and its application in capacitive deionization and energy storage. *Biomass Bioenergy* **2016**, *87*, 107–121. [CrossRef]
54. Jagtoyen, M.; Derbyshire, F. Activated carbons from yellow poplar and white oak by H_3PO_4 activation. *Carbon* **1998**, *36*, 1085–1097. [CrossRef]
55. Mandal, A.; Singh, N.; Purakayastha, T.J. Characterization of pesticide sorption behaviour of slow pyrolysis biochars as low cost adsorbent for atrazine and imidacloprid removal. *Sci. Total Environ.* **2017**, *577*, 376–385. [CrossRef]
56. Torrellas, S.Á.; Lovera, R.G.; Escalona, N.; Sepúlveda, C.; Sotelo, J.L.; García, J. Chemical-activated carbons from peach stones for the adsorption of emerging contaminants in aqueous solutions. *Chem. Eng. J.* **2015**, *279*, 788–798. [CrossRef]
57. Fu, J.; Chen, Z.; Wang, M.; Liu, S.; Zhang, J.; Zhang, J.; Han, R.; Xu, Q. Adsorption of methylene blue by a high-efficiency adsorbent (polydopamine microspheres): Kinetics, isotherm, thermodynamics and mechanism analysis. *Chem. Eng. J.* **2015**, *259*, 53–61. [CrossRef]
58. Gong, J.; Liu, J.; Chen, X.; Jiang, Z.; Wen, X.; Mijowska, E.; Tang, T. Converting real-world mixed waste plastics into porous carbon nanosheets with excellent performance in the adsorption of an organic dye from wastewater. *J. Mater. Chem. A* **2015**, *3*, 341–351. [CrossRef]
59. Ai, L.; Zhang, C.; Liao, F.; Wang, Y.; Li, M.; Meng, L.; Jiang, J. Removal of methylene blue from aqueous solution with magnetite loaded multi-wall carbon nanotube: Kinetic, isotherm and mechanism analysis. *J. Hazard. Mater.* **2011**, *198*, 282–290. [CrossRef]
60. Fan, S.; Wang, Y.; Wang, Z.; Tang, J.; Tang, J.; Li, X. Removal of methylene blue from aqueous solution by sewage sludge-derived biochar: Adsorption kinetics, equilibrium, thermodynamics and mechanism. *J. Environ. Chem. Eng.* **2017**, *5*, 601–611. [CrossRef]
61. Fan, S.; Tang, J.; Wang, Y.; Li, H.; Zhang, H.; Tang, J.; Wang, Z.; Li, X. Biochar prepared from co-pyrolysis of municipal sewage sludge and tea waste for the adsorption of methylene blue from aqueous solutions: Kinetics, isotherm, thermodynamic and mechanism. *J. Mol. Liq.* **2016**, *220*, 432–441. [CrossRef]

62. Leng, L.; Yuan, X.; Huang, H.; Shao, J.; Wang, H.; Chen, X.; Zeng, G. Bio-char derived from sewage sludge by liquefaction: Characterization and application for dye adsorption. *Appl. Surf. Sci.* **2015**, *346*, 223–231. [CrossRef]
63. Du, X.-D.; Wang, C.-C.; Liu, J.-G.; Zhao, X.-D.; Zhong, J.; Li, Y.-X.; Li, J.; Wang, P. Extensive and selective adsorption of ZIF-67 towards organic dyes: Performance and mechanism. *J. Colloid Interface Sci.* **2017**, *506*, 437–441. [CrossRef] [PubMed]
64. Gong, J.; Liu, J.; Jiang, Z.; Wen, X.; Mijowska, E.; Tang, T.; Chen, X. A facile approach to prepare porous cup-stacked carbon nanotube with high performance in adsorption of methylene blue. *J. Colloid Interface Sci.* **2015**, *445*, 195–204. [CrossRef] [PubMed]
65. Fan, S.; Wang, Y.; Li, Y.; Tang, J.; Wang, Z.; Tang, J.; Li, X.; Hu, K. Facile synthesis of tea waste/Fe_3O_4 nanoparticle composite for hexavalent chromium removal from aqueous solution. *RSC Adv.* **2017**, *7*, 7576–7590. [CrossRef]